Dalton Transactions

Accepted Manuscript

ROYAL SOCIETY OF CHEMISTRY

www.rsc.org/dalton

The usefulness of EPR spectroscopy in the study of compounds with metal–metal multiple bonds*

Naresh S. Dalal[†,‡] and Carlos A. Murillo[†,§]

Department of Chemistry, P.O. Box 30012, Texas A&M University, College Station, Texas 77842-3012 and University of Texas at El Paso, El Paso, Texas 79968 and

Department of Chemistry and Biochemistry, and National High Magnetic Field, Florida State University, Tallahassee, Florida, 32306-4390

* Electronic supplementary information (ESI) available: Basic EPR background.

† To whom correspondence should be addressed: dalal@chem.fsu.edu (NSD), murillo@tamu.edu (CAM)

‡ Florida State University

§ Texas A&M University and University of Texas at El Paso

Synopsis graphic and text

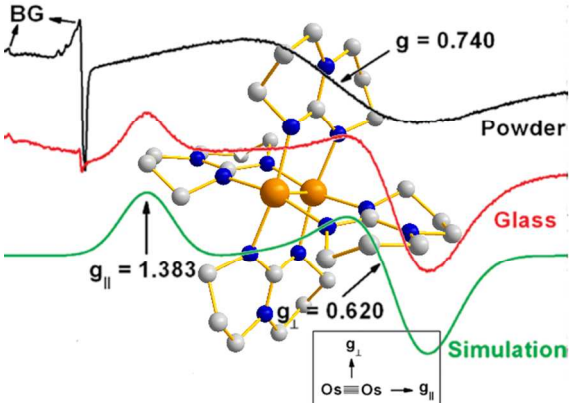

A discussion of how EPR spectroscopy has contributed to the understanding of the electronic structure of paddlewheel compounds with multiple bonds between metal atoms is presented while commemorating the 50th anniversary of the paper describing the quadruple bond and the identification of the delta bond in the $Re_2Cl_8^{2-}$ anion.

Abstract

This Perspective reviews some of the contributions that EPR spectroscopy has made for the understanding of the bonding and electronic structure of molecular species with metal-to-metal multiple bonds. A goal is to show how useful this technique can be in (a) elucidating whether unpaired electrons reside in metal-based or ligand-based molecular orbitals, (b) providing information on the metal center's total electronic spin, an aspect that offers support to its oxidation state, (c) informing about the distribution of the unpaired electrons between the metals and the organic ligand, (d) detecting molecular dynamics and phase transitions to complement X-ray studies and (e) using high-frequency, high-field EPR for studying compounds that might be EPR-silent when only commonly

available spectrometers are used. A brief comparison with NMR is provided in the electronic supporting information where it is noted that for typical laboratory magnetic fields, the energy gap between resonant states in EPR is in the microwave region of the electromagnetic spectrum (GHz) while for NMR it is in the radiofrequency range (MHz). Our aim is to encourage the inorganic chemistry community and more broadly other chemists and physicists to collaborate while characterizing new paramagnetic inorganic complexes. Enough basic background is provided as supplementary material to allow senior-level undergraduate and graduate students to understand the simplicity as well as the power of EPR spectroscopy with the view of encouraging them to use this technique in their own research activities. Finally, it should be noted that this report commemorates the fiftieth anniversary of the description in *Science* of the first species with a quadruple bond that is given in reference 1.

1. Introduction

Fifty years ago, Inorganic Chemistry saw the advent of an influential paper that revolutionized the field of compounds with metal-to-metal bonds. This paper in *Science* described the quadruple bond in the anion $Re_2Cl_8^{2-}$, a species with a Re–Re distance of 2.24 Å that is significantly shorter than that in rhenium metal (ca. 2.50 Å).[1] This anion has D_{4h} symmetry and thus the chlorine atoms are eclipsed as shown in Fig. 1. In the germinal paper, the eclipsed configuration was attributed to the presence of a delta bond. Because each of the metal atoms has four metal-based electrons, the electronic configuration for this dinuclear species can be written as $\sigma^2\pi^4\delta^2$ which is abbreviated as Q. The molecular orbitals (MOs) are formed by overlap of dz^2, d_{xz}, d_{yz} and d_{xy} orbitals from each metal atom where the z direction coincides with the metal–metal bond axis. Because the four ligands in each metal atom occupy a set of dx^2-y^2 hybrid orbitals,[2] these are not available for metal-to-metal bonding and thus when there are additional electrons, these occupy antibonding MOs and the bond order decreases. As a first approximation the MO diagram shown in Fig. 2 with an ordering of $\sigma < \pi << \delta < \delta^* < \pi^* < \sigma^*$ can be used to represent the various configurations.[3]

After the discovery of $Re_2Cl_8^{2-}$ a flurry of activity led to the syntheses of $Re_2X_8^{2-}$ analogues and this was then followed by replacement of the halide atoms by bridging, anionic ligands such as carboxylates ($RCCO_2$), amidinates (RNC(R′)NR), guanidinates (characterized by the NC(N)N cores) and others.[3] Several additional transition metal atoms have been used to synthesize a large number of metal–metal bonded compounds. These species with two (and sometimes more) metal atoms spanned by four bridging mononegative bidentate ligands are often referred to as paddlewheel compounds because of their resemblance to the wheel in old steam-powered river-boats.[4]

From the MO diagram in Fig. 2, it is evident that in quadruple bonded species having eight metal-based electrons all electrons are paired. Therefore these compounds are diamagnetic. However, one electron oxidation or reduction processes produce species with unpaired electrons, termed paramagnetic, which can be best studied by EPR (electron paramagnetic resonance) spectroscopy.[5] In this Perspective a selection of the work done in our laboratories will be presented. Work from other laboratories will not be dealt with in detail. Appropriate references can be found in ref. 3. The main objective is to show how EPR, an uncommonly used tool, can provide invaluable information often unattainable with other techniques and how various experimental techniques may complement each other.

Most paramagnetic paddlewheel compounds have only one unpaired electron (S = ½) that leads to a fractional bond order, exceptions being those species with two electrons in π* orbitals (S = 1) and those with $\pi^{*2}\delta^*$ electronic configurations (S = 3/2). For these compounds one of more important questions that EPR has been able to answer is whether the unpaired electron after a reduction or an oxidation process of a diamagnetic species is in a metal-based MO or in a ligand-based orbital.

2. Compounds with $\sigma^2\pi^4\delta$ electronic configurations

2.1 Mo_2^{5+} tetracarboxylates

Most of these compounds are obtained by oxidation of species with a bond order (b. o.) of 4. Examples studied are those of the relatively unstable and somewhat difficult to stabilize $[Mo_2(RCOO)_4]^+$ species, where the carboxylate is either butyrate[6] or 2,4,6-triisopropylphenyl carboxylate (TiPB).[7] The one-electron electrochemical oxidation (Mo_2^{4+}/Mo_2^{5+}) of $Mo_2(TiBP)_4$ in dichloromethane, ethanol, and acetonitrile exhibits values for $E_{½}$ of +0.621, +0.448, and +0.462 V (vs Ag/AgCl), respectively. For the butyrate analogue the trend is similar ($E_{½}$ values of +0.45, +0.30, and +0.39 V vs SCE). Two oxidized $[Mo_2(TiBP)_4]X$ species, X = PF_6 and BF_4, have been isolated. Upon removal of an electron the formal bond order is reduced from 4 to 3.5 and consistently the Mo–Mo bond distance elongates by about 0.05 Å from 2.076(1) Å to 2.1364(8) and 2.1441(5) Å for $Mo_2(TiBP)_4$, $[Mo_2(TiBP)_4]PF_6$ and $[Mo_2(TiBP)_4]BF_4$, respectively. Magnetic measurements using a SQUID magnetometer are consistent with the presence of one unpaired electron over the range of 300 to 2 K. The X-band EPR spectrum shown for the PF_6 analogue has a signal that displays both the parallel and perpendicular components as expected from a species with the idealized tetragonal symmetry of a paddlewheel. It also shows hyperfine structure attributed to the interaction of the $^{95/97}$Mo (I = 5/2) isotopes ($g_{\parallel} = g_{\perp} = 1.936$, $A_{\parallel} = 35.60 \times 10^{-4}$ cm^{-1}, and $A_{\perp} = 18.20 \times 10^{-4}$ cm^{-1}),[8] constituting direct evidence of the existence of a Mo–Mo bond in this complex. It is noteworthy that, in several of these complexes, while the g-tensor is isotropic, the hyperfine coupling is distinctly anisotropic.

2.2 Mo_2^{5+} formamidinates

Similarly oxidation of $Mo_2(DAniF)_4$ (DAniF = *N*,*N*′-di-*p*-anisylformamidinate) with $[Fe(Cp)_2]PF_6$ and subsequent replacement of the hexafluorophosphate by the anion tetra-3,5-bis(trifluoromethyl)phenylborate (TFPB) produces an elongation of the Mo–Mo distance of about 0.04 Å to 2.1373(6) Å.[9] The X-band EPR spectrum of a CH_2Cl_2 solution at ambient temperature shown in Fig. 3[10] has an isotropic g value, g_{iso}, of 1.948 and a hyperfine, A, value of 22×10^{-4} cm^{-1}. The g value of significantly less than 2.00,[11] coupled with the relatively broadness of the EPR band and more

importantly the hyperfine values are consistent with the unpaired electron being in a metal-based MO. In the spectrum in Fig. 3, the larger peak is derived from the more abundant even-even $I = 0$ isotopes, while the weaker hyperfine pattern of splittings is consistent with the presence of $I = 5/2$ nuclei (the hyperfine weakness is commensurate with the smaller natural abundance of the underlying nuclei). The overall pattern constitutes positive confirmation of the assignment.

2.3 Mo_2^{5+} tetrasulfate and tetrahydrophosphate

One of the earliest Mo_2^{5+} species is that in the $[Mo_2(SO_4)_4]^{3-}$ anion for which $g_{\parallel} = 1.891$ and $g_{\perp} = 1.901$.[12] Similarly for the hydrophosphate (HPO_4^{2-}) analogue $g_{\parallel} = 1.886$ and $g_{\perp} = 1.894$.[13]

2.4 Cr_2^{5+} species

An illustration of a compound that required the use of high field to unambiguously determine where the unpaired electron is located is that of $\{Cr_2[(DPPC)_4]_4\}PF_6$ where DPPC is the guanidinate ligand $(PhN)_2CN(CH_2)_4$ (Scheme 1).[14] In this ligand each of the equivalent N atoms is bound to a phenyl group and the unique nitrogen atom is part of a 5-membered heterocyclic ring having 4 methylene groups. At X-band, the spectrum shows a single slightly broad signal devoid of hyperfine structure with a g ~2.00. The Cr–Cr distance of 1.9249(9) Å is only slightly longer than that of 1.904(1) Å in the neutral molecule. With this information, an unambiguous assignment of whether this is a metal-based or a ligand-based oxidation is difficult. However, further studies done at X-band (9.5 GHz) using a crystalline sample at 300 K provided sufficient information pointing to a metal-based oxidation. The top portion of Fig. 4 shows the X-band (9.5 GHz) spectrum with an internal standard of the organic radical DPPH (DPPH = 2,2-diphenyl-1-picrylhydrazyl). The dichromium complex has a relatively broad band with a g value of 1.973 that is smaller than that of the DPPH radical (2.0037). More importantly, upon increasing the frequency to W-band (95 GHz), the band is split and there are g values of $g_{\parallel} = 1.9701 \pm 0.0005$ and $g_{\perp} = 1.9767 \pm 0.0005$. This pattern is what would be expected from a species with an approximately cylindrical

symmetry. Importantly, these values are consistent with the observed isotropic X-band value of g_{iso} = 1/3($g_{\parallel}$ + 2$g_{\perp}$) = 1.975.[15]

An interesting comparison was possible when the spectra for $[Mo_2(TiBP)_4]PF_6$ were obtained at W-band.[14b] As seen in Fig. 5, the ambient temperature spectrum is less resolved than that taken at 10 K which shows three *g* values (one along each of the Cartesian coordinates, g_x, g_y and g_z). The appearance of three *g* values shows that a lowering of the symmetry from tetragonal to rhombic takes place upon lowering the temperature.

2.5 V_2^{3+} species

Another compound with a bond order of 3.5 contains a rare V_2^{3+} core and is obtained by reduction of the triple bonded $V_2(DPhF)_4$ compound (DPhF = *N*,*N*′-diphenylformamidinate).[16] The spectrum obtained using a frozen THF glass at 6 K is shown in Fig. 6. The multiline spectrum is consistent with the unpaired electron being coupled with each ^{51}V (*I* = 7/2, ~100%) nucleus equally.[16b,17] A simulation of the main feature gave a *g* of 1.9999. Although this value is close to that of the free-electron, the complex hyperfine splitting pattern indicates that much of the electron density from the unpaired electron is localized on the dimetal core.

2.6 Re_2^{5+} species

Finally, it should be mentioned that there are a number of complexes obtained by reduction of quadruple bonded Re_2^{6+} compounds that have Re_2^{5+} cores. This core possesses the so-called electron rich bond of order 3.5 where the unpaired electron is in a δ* antibonding orbital ($\sigma^2\pi^4\delta^2\delta^*$) rather than in a bonding δ orbital ($\sigma^2\pi^4\delta^1$).[3,18]

2.7 Re_2^{7+} compounds with bicyclic guanidinates

An important group of ligands that have been used in one of our laboratories is that of the bicyclic guanidinates, one of which is shown in Scheme 1. These ligands are characterized by having the NC(N)N moiety embedded in two cyclic units. Perhaps the most important property they have is their ability to

destabilize electrons in δ-type orbitals[19] which leads to extremely facile removal of such electrons and the formation of dimetal units is unusually high oxidation states, many of which act as very strong reducing agents and have ionization energies less than that of the cesium atom.[20]

With the use of bicyclic guanidinates the first oxidation of the well-known quadruple bonded Re_2^{6+} species was observed. This produces Re_2^{7+} cores with a presumed $\sigma^2\pi^4\delta$ electronic configuration. The first such compound to be studied by EPR was $[Re_2(hpp)_4Cl_2]PF_6$.[21] The challenge here was to determine whether the unpaired electron was in a metal-based MO. Initially there were doubts since an increase in the positive charge of the metal atoms may lead to sufficient repulsion and contraction of the atomic orbitals that could prevent metal-to-metal bonding. The X-band EPR spectrum (Fig. 7) at ambient temperature of a powder consists of a single exchange-narrowed featureless line with a peak-to-peak line width of 600 G at g = 1.7421; i.e., the hyperfine pattern is averaged out by the electron-electron spin exchange. This g-value is in reasonably good agreement with that obtained from the Curie-Weiss fit (g = 1.696) from magnetic susceptibility data,[22] suggesting that the location of the unpaired electron is on the metal atoms. Because more definitive evidence was desirable to support that the electron was on metal-based MOs, measurement of hyperfine interaction were pursed. During this process a very dramatic spectral resolution improvement was observed when the sample was dissolved in CH_2Cl_2 (10 mM) and the spectrum collected in a sealed-tube above ambient temperature (340 K, see Fig. 8). The dilution reduced the solid-state effects (dipolar and magnetic exchange) providing a relatively well-resolved spectrum. The hyperfine structure arises from the two natural isotopes: ^{185}Re, 37.4% abundance, g_n = 1.2748, I = 5/2 and ^{187}Re, 62.6% abundance, g_n = 1.2878, also with I = 5/2, both having approximately the same hyperfine coupling constants within the experimental resolution, as expected from the near equality of their nuclear g_n-values. The presence of 11 hyperfine lines[17] indicates that the unpaired spin is (essentially) equally distributed on the two equivalent Re ions in the Re_2^{7+} core. The spectrum is not fully isotropic even at elevated temperatures, which has been attributed to the

relatively slow tumbling of the heavy molecules with bulky ligands. From the spectral simulation at elevated temperatures, the parameters g_{iso} = 1.7535 ± 0.0002 and A_{iso} = 283 ± 5 G (695 MHz) have been obtained. The large deviation from g = 2 is due to spin-orbit coupling in the heavy Re ions and indicates that the oxidation is metal-based rather than ligand-based.

Further evidence was obtained when the frequency was increased from 9.5 GHz to 34.5 GHz (Q-band) the resolution of the spectrum for the frozen CH_2Cl_2 glass at 153 K increased even further, as seen in Fig. 9. The spectrum consists of 33 lines, superimposed on one another to some extent. Interestingly when the frequency was increased further to 90 GHz (W-band) a spectral degradation was observed. The spectrum is less resolved because of the greater g-strain and hence larger line widths at higher Zeeman fields. Because of the large g-tensor anisotropy in this compound, the Q-band spectra yielded the optimum combination of spectral resolution and intensity. The Q-band data provided full tensors for both the g-factor and the hyperfine interaction;[19] the isotropic averages of the frozen solution data agreed well with those from the fluid solution studies. The dipolar part of the hyperfine tensor provided a direct measure of the unpaired electron spin density in the metal d-orbitals; the data clearly demonstrated that the unpaired electron in the $[Re_2(hpp)_4Cl_2]^+$ cation is in an MO of predominant metal character with little mixing from the guanidinate ligands. This example emphasizes the value of using multifrequency EPR coupled with variable temperature solution phase measurements.

3. Electron-rich bond order of 3.5

3.1 Os_2^{7+} species

A species with an unpaired electron in a δ* orbital is that having an Os_2^{7+}core. Indeed the first species with an M_2^{7+} core to be studied by EPR was $[Os_2(hpp)_4Cl_2]PF_6$.[23] At 6.5 K this compound yielded what at the time was considered to be a very unusual EPR spectrum of the solid (Fig. 10) since it had a quite atypical low g value of 0.791 ± 0.037. Additionally the observed peak-to-peak line width (~6000 G) is exceptionally large. Now we can attribute this to dipolar coupling between paramagnetic centers

coupled with fast electronic relaxation time. This line width can be contrasted with the sharpness of the signal from the free radical α,γ-bisdiphenylene-β-phenylallyl (BDPA) at g = 2.0035. A few years later further investigations using single crystals, solution and frozen solutions were carried out.[24] They provided a better understanding of the unusual spectrum as summarized below.

When solutions of $[Os_2(hpp)_4Cl_2]PF_6$ in CH_2Cl_2 (~0.06 M) were used, no signal was detectable above 175 K, indicating the spin-lattice relaxation time was very short. However, spectra were obtained upon freezing the solution to temperatures below 50 K, as shown in Fig. 11b. The spectra consist of two clearly resolved peaks, labeled $g_{\parallel}$ and $g_{\perp}$, characteristic of a randomly oriented S = ½ paramagnetic compound with axial symmetry, but without any hyperfine interaction. The assignment of $g_{\parallel}$ and $g_{\perp}$ (vide infra) has been made using what is customary for axially-symmetric paramagnetic complexes, with the peak labeled $g_{\parallel}$, arising from those molecules whose principal symmetry axis is oriented along the applied field H, while that for $g_{\perp}$ corresponding to those oriented with their four-fold symmetry axes lying perpendicular to H. Fig. 11c presents the simulation of the frozen glass EPR spectrum of Fig. 11b, assuming $g_x = g_y = g_{\perp}$ and $g_z = g_{\parallel}$. The best-fit parameters are $g_{\parallel}$= 1.383 ± 0.004 and $g_{\perp}$ = 0.620 ± 0.002. Because the Os–Os bond represents the principal axis of symmetry in $[Os_2(hpp)_4Cl_2]PF_6$, $g_{\parallel}$ corresponds to the Os–Os bond direction, and $g_{\perp}$ lies in the plane perpendicular to the direction of the Os–Os bond, as shown in the inset of Fig. 11. In addition, the averaged g value $[g_{\parallel}/3 + (2 \times g_{\perp})/3]$ of 0.874 is close to that of the powder spectra (0.740). The value for the g anisotropy Δg = 1.383 – 0.620 = 0.763 is significantly larger than that of mononuclear Os compounds and other d^5 species. The directions of the $g_{\parallel}$ and $g_{\perp}$ components relative to the molecular structure of $[Os_2(hpp)_4Cl_2]PF_6$ were determined using single crystals. These were rectangular plates, and X-ray studies established that the crystal plate corresponds to the $1\bar{1}0$ plane of the unit cell, as shown in Fig. 12. The EPR spectra were obtained at 4.5 K by orienting the crystal relative to the magnetic field at 10° intervals, as shown in Fig. 13. From crystallographic data shown in Fig. 12, it can be seen that the Os–Os bonds of the two magnetically

independent molecules are oriented at approximately 8.835° from the *ab* plane (001), which means that the Os–Os bonds are nearly parallel to the *ab* plane. In general, the spectra should consist of two peaks for the two orientations of Os–Os bonds, but only one peak when the two peaks merge into one at an angle of about 100°. This only happens when the magnetic field is perpendicular to the *ab* plane (001) and is almost perpendicular to all of the Os–Os bonds. The measured *g* value using this approximation was 0.808 which is close to $g_{\perp}$ = 0.620, indicating that $g_{\perp}$ corresponds to the perpendicular direction of Os–Os bond, and $g_{\parallel}$ lies along the Os–Os bond direction. This description is in accordance with the idealized D_{4h} symmetry of $[Os_2(hpp)_4Cl_2]PF_6$ about the Os–Os bond and with the prediction of the simulations of the frozen glass spectra.

The observed EPR line width of ~3775 G cannot at all arise from an unpaired electron localized on an organic radical (either carbon- or nitrogen-centered), because the expected line width for an organic radical is at most 40–50 G. Facts, such as the excessively large line width and the signal being observable only below about 50 K, imply that the spin-lattice relaxation time, T_1, of the Os_2^{7+} center is very short—an observation that again is incompatible for an organic radical. An upper limit on the magnitude of T_1 can be obtained from the relationship $T_1 = \hbar/g\beta\Delta H$, where ΔH is the experimental line width. Using ΔH ≈ 3 775 G and *g* = 0.740, the value of $T_1 \approx 4 \times 10^{-11}$ s is obtained. Such a short excited-state lifetime, T_1, strongly supports that the unpaired electron resides preferentially in a δ* orbital rather than a π* orbital. These results are also in agreement with those in the only other M_2^{7+} species known, namely the Re_2^{7+} analogues mentioned above. These compounds also have a formal bond order of 3.5, but there is an important distinction in that the electronic configuration differs from that of $[Os_2(hpp)_4Cl_2]PF_6$ since in the rhenium species, the configuration is the electron poor $\sigma^2\pi^4\delta$ that results from removal of an electron from a bonding δ orbital of the quadruple bonded precursor $Re_2(hpp)_4Cl_2$ while that in $[Os_2(hpp)_4Cl_2]PF_6$ is the electron rich $\sigma^2\pi^4\delta^2\delta^*$.

3.2 Tc_2^{5+} compounds

The first species studied by EPR with an electron-rich b. o. of 3½ and a $\sigma^2\pi^4\delta^2\delta^*$ electronic configuration was that in $[Tc_2Cl_8]^{3-}$.[25] To preclude solid-state effects the EPR measurements were made on frozen solutions at X and Q-band. The spectra show extensive hyperfine structure due to coupling of two equivalent ^{99}Tc (I = 9/2) nuclei with of $g_{\|}$ = 1.912 and $g_{\perp}$ = 2.096, $A_{\|}$ = 1.66 × 10^{-4} cm^{-1} and $A_{\perp}$ = 67.2 × 10^{-4} cm^{-1}. As discussed above, these values are consistent with the unpaired electron being primarily in a metal-based MO. Importantly, the variation of the Tc–Tc bond distance with respect to the bond order is unusual since there is a decrease in the distance from 2.147(4) Å[26] to 2.117(2) Å in $M_3Tc_2Cl_8{\cdot}nH_2O$, M = K, Y,[27] and 2.13(1) Å in $(NH_4)_3Tc_2Cl_8{\cdot}2H_2O$.[28]

3.3 Ni_2^{5+} species

EPR spectroscopy has also been useful in the study of species with 15 metal-based electrons and a b. o. of ½. In $[Ni_2(DTolF)_4]BF_4$ which is obtained by reduction of the parent $Ni_2(DAniF)_4$ species (DAniF = *N*,*N*′-di-p-anisylformamidinate).[29] In the neutral species the divalent Ni atoms have a closed-shell d^8 configuration and there is no metal-metal bond. Upon electrochemical and chemical oxidation, the non-bonded Ni···Ni separation of 2.476 (1) Å decreases to 2.3703(4) Å. The product is EPR active. The $g_{\perp}$ component appears at 2.234 and the $g_{\|}$ component at 2.045. The latter is partly overlapped by a somewhat broad, structureless signal at about g = 2.0. Again the large deviation of the anisotropic g-value components from 2.00 and absence of Zero-field splitting clearly establishes the presence of one unpaired electron on the Ni_2^{5+} core.

3.4 Pd_2^{5+} species

Another species with a b. o. of ½ is found in the Pd_2^{5+} analogue, $[Pd_2(DTolF)_4]PF_6$. Upon oxidation of the precursor, the Pd–Pd distance decreases by 0.052 Å from 2.6486(8) to 2.597(1) Å but the X-band EPR shows only a broad, featureless band with g = 2.01 which resembles somewhat that in organic radicals with a g of 2.00. However, high field EPR spectroscopy again supports that the unpaired electron is in metal-based MOs since the anisotropy is clearly observed as the microwave frequency increases from

9.6 to 34.06 to 105.6 to 211.2 GHz as seen in Fig. 14.[30] This is another clear example of the usefulness of using various field strengths. As usual, the large increase in line width at elevated temperatures originates from the life-time (spin-lattice relaxation) processes. Such a short spin-lattice relaxation time can only arise from a metal-containing paramagnetic species. The spectrum at 10 K implies that there are three *g* values (g_x = 2.0367, g_y = 2.0134, and g_z = 1.9971). Because there are three *g* components this suggests there is rhombic symmetry (not tetragonal symmetry found in the crystal structure determined from data collected at 213 K). It is therefore possible that at low-temperature a structural and crystallographic phase transition takes place. Unfortunately this hypothesis has not been tested since low temperature X-ray studies have not been done on this compound.

3.5 Ir_2^{5+} and Co_2^{5+} compounds

Finally, there is an Ir_2^{5+} species in $Ir_2(DAniF)_4(O_2CCF_3)$ that has an Ir–Ir bond distance of 2.5073(9) Å.[31] The EPR spectrum of a frozen solution in CH_2Cl_2 at –100 °C is consistent with an unpaired electron and a state of S = ½. The g_{iso} is 2.14. An analogous Co_2^{5+} species in $[Co_2(PhNC(Ph)NPh)_4]^+$ shows a signal at g = 1.98 that is split into 15 equally spaced lines derived from the two cobalt atoms, each with I = 7/2, showing the MO of the unpaired electron to be metal-centered.[32] As noted before, the number of hyperfine peaks (15 here) and their relative intensities (1:2:3:4:5:6:7:8:7:6:5:4:3:2:1) are diagnostic of the number and nuclear spins of the nuclei electron.[17]

4. The Complex Situation in Diruthenium Compounds

Compounds with Ru_2^{n+} units are known having n = 4, 5 and 6.[3] The electronic configurations can be quite complex since often cross-over is possible and evidence of large Zero-splitting is frequently encountered.[33] In addition, it is not unusual that δ* and π* orbitals have similar energies. It is also possible that for certain configurations there might be two unpaired electrons, e. g., δ*π*, π*δ*, π^{*2} and thus S = 1. These type of electronic configurations often are EPR silent and thus EPR spectroscopy is

not as useful as in the examples discussed above. Because of this relatively few EPR studies on diruthenium species have been done.

One compound that has been studied is $Ru_2(D(3,5\text{-}Cl_2Ph)F)_4Cl$.[34] This has a Ru_2^{5+} core with 11 metal electrons and a formal b. o. of 2.5 (D(3,5-Cl_2Ph)F = *N*,*N*′-3,5(dichlorophenyl)formamidinate). The compound has a $^4B_{2u}$ ground state derived from a $\sigma^2\pi^4\delta^2\pi^{2*}\delta^*$ electronic configuration and thus there are 3 unpaired electrons. The persistence of this configuration from 27 to 300 K was established by the variable temperature crystallographic study that showed invariance of the Ru–Ru distance. Orientation-dependent magnetic susceptibility (χT) and magnetization (M(H)) data are in accord with a spin quartet ground state with large magneto-crystalline anisotropy associated with a large axial Zero-field splitting (D) parameter. Theoretical fits to χT and M(H) plots yielded D/k_B = +114 K, implying an $S = \pm ½$ Kramers doublet ground state at low temperature. Single-crystal and powder EPR data are consistent with this result, as the only observed transition is between the $M_s = \pm ½$ Zeeman levels. The *g* values are $g_\perp$ = 2.182, g_{II} = 1.970, and D = 79.8 cm^{-1}. The totality of the results demands D much greater than 0. This was probably the first direct proof of D being very large and while having a positive value for this class of compounds.[32] An electronic splitting diagram for this 11 metal-centered species with idealized D_{4h} symmetry is given in Scheme 2. It is worth noting that usually for these compounds with $S = 3/2$ and a large Zero-field splitting, the observed spectra are characterized by the 'effective' *g*-values, $g_\perp \sim 4$ and $g_{II} \sim 2$, but with the real *g*-values as stated (2.182 and 1.970, respectively).[35]

Another compound examined by EPR is $[Ru_2(C_3H_7COO)_4]Cl$.[36] The frozen methanol solution at 77 and 4.2 K gave $g_\perp = 2.1 \pm 0.1$ and $g_{II} = 2.18$. A hyperfine pattern was observed only at 4.2 K and was interpreted in terms of coupling of two equivalent nuclei, where $A_{II} = (9 \pm 3) \times 10^{-3}$ cm^{-1} and $A_\perp = (31 \pm 1) \times 10^{-4}$ cm^{-1}.

5. *Pairs-of-pairs*

There is a voluminous literature on compounds with two or more dimetal units bound by various linkers.[37] The simplest units contain two dimetal units joined together by a linker and these are referred to as *pairs-of-pairs*. Because of the resemblance to the Creutz-Taube ion,[38] these *pairs-of-pairs* have been interrogated by electrochemical, crystallographic, and other spectroscopic methods including EPR with the idea of determining if the two dimetal units communicate through the linker.

5.1 A tetramethoyzincate linker

Some of the first *pairs-of-pairs* to be studied by EPR spectroscopy contained the tetrazincate cations $[(DAniF)_3Mo_2(OCH_3)_2Zn(OCH_3)_2Mo_2(DAniF)_3]^{n+}$, n = 1, 2.[39] The structure shows that the two dimetal units, consisting of $Mo_2(DAniF)_3$ units, are essentially perpendicular to each other and they are held together by a bridging $Zn(OCH_3)_4^{2-}$ anion. Importantly, upon oxidation of the neutral compound one of the Mo–Mo bond distances increases while the other one remains essentially unchanged (2.151(1) and 2.116(1) Å). However, when the second oxidation process takes place, giving a species with two dimetal units with bond orders of 3.5, both of the crystallographically independent Mo–Mo distances are essentially the same (2.147(1) and 2.151(1) Å). This suggests that there is little electronic communication between the two units producing localization of the unpaired electrons and this is consistent with a small comproportionation constant, K_C.[40] This result is also consistent with the fact that the dimetal units are essentially perpendicular to each other. The X-band EPR spectrum in Fig. 15 is very similar to that for $[Mo_2(TiPB)_4]PF_6$[Error! Bookmark not defined.] and $[Mo_2(DAniF)_4]PF_6$ (Fig. 3).[9] The doubly oxidized compound has two unpaired electrons and an EPR spectrum very similar to the previous ones (e. g., Fig. 3). This strongly indicates that the unpaired electrons are localized.

5.2 An isomer pair

Further evidence of how EPR can complement the determination of whether an unpaired electron in a *pair-of-pairs* is localized or delocalized in the dimetal units can be obtained by studying the hyperfine structure in the spectra as manifested in the *A* value. An unambiguous example is provided by an isomer

pair composed of two $(DAniF)_3Mo_2$ units linked by a diaryloxamidate.[41] As shown in Fig. 16 in one of the compounds, the two dimetal units are essentially perpendicular to each other (α isomer), while in the other the two dimetal units are essentially parallel (β isomer.) For these species, six compounds have been isolated: two neutral quadruple bonded species, two single oxidized and two double oxidized. The K_C for the α species is only 10^3 while that for the β is 10^6. The X-ray crystallographic data show two distinct Mo–Mo distances for the α^+ species that differ by about 0.04 Å but they are essentially the same in the β^+ species. This β^+ species also displays a HOMO–1 → SOMO transition at 4700 cm^{-1} ($\Delta\nu_{½}$ = 2300 cm^{-1}) while there is no band in this region for the α^+. These data strongly suggest that in the mixed-valent α^+ species the unpaired electron is localized over only one of the Mo_2 units while in the β^+ cation the unpaired electron is delocalized over the two Mo_2 units. In addition, the α^{2+} behaves as a diradical having two Mo_2^{5+} units that are essentially uncoupled while the β^{2+} species is diamagnetic. The EPR data are also consistent with this assignment. While the *g* values are similar: 1.950, 1.947 and 1.951 for α^+, β^+ and α^{2+}, respectively, the *A* values are quite different. For the species with localized unpaired electrons (α^+ and α^{2+}) the hyperfine *A* value is 21×10^{-4} cm^{-1} while for the species with the delocalized unpaired electron (β^+) *A* becomes nearly one half: (11×10^{-4} cm^{-1}). Importantly, the same values are observed for many other pairs-of-pairs having dimolybdenum units with an unpaired electron.[42] Thus these values can be used as an effective measure of electronic localization/delocalization in *pairs-of pairs* with dimolybdenum units.

6. An example of an EPR-silent species: Unique value of HF-EPR

Finally we mention an instructive example of related paramagnetic complexes on which EPR measurements using X-band or even Q-band spectrometers may not yield a signal, but high field (HF-EPR) measurements will likely do. One of the best examples of an extended paddlewheel complex that was considered to be EPR silent is $Cr_3(dpa)Cl_2$, an extended metal atom chain (EMAC) having a linear trichromium unit wrapped by four dipyridylamido ligands derived from Hdpa (Scheme 1). In this species

each terminal chromium atom is also bound to a chlorine atom positioned in an axial location as shown in Fig. 17. This $Cr_3(dpa)_4Cl_2$ compound has a Cr_3^{6+} core in which each metal atom is divalent.[43] The three chromium atoms are antiferromagnetically coupled, leaving a total of 4 unpaired electrons on the unit, with spin S = 2. From basic principles, one would thus expect at least $2S$ = 4 EPR transitions for each symmetry direction of the molecule, and a total of 8 for a powder sample if the molecule has axial or three-fold symmetry, and 12 for that with lower than three-fold point symmetry. However, this compound is EPR-silent from measurements done at X-band at 10 K.[44] Additional studies at Q-band spectra yielded additional features which could be ascribed to a single molecule with three different *g*-tensor components, but clearly insufficient to determine the full spin-Hamiltonian parameters. One possibility was that the material itself might be EPR-silent and the observed signal could be attributed to an impurity perhaps from a decomposed product. Another proposal was that the *D*-value of the complex is so large that the X-band or Q-band microwave quanta are too small to induce most of the EPR transitions. As shown in Fig. 18 this proposal turned out to be correct since measurements at higher frequencies, up to 400 GHz,[45] yielded the expected number of peaks for an S = 2 complex, with a large Zero-field splitting of –1.64 cm^{-1} (~ 50 GHz). This frequency/field of 400 GHz/12 T is much larger than available with most commercial EPR spectrometers demonstrating the usefulness of HF-EPR for some important metal-metal bonded complexes.

7. Summary

The main focus of this perspective was to illustrate how modern EPR techniques have aided the understanding of the bonding and electronic structure of dimetal paddlewheel complexes. This field that began 50 years ago with the report of the $Re_2Cl_8^{2-}$ anion, and its variants, and has since mushroomed into a mature field. Nevertheless there were important unanswered questions on the electronic structure of species with fractional bond orders. Relevant questions remained on whether the bonding between the metals was actually of the covalent–type, and on their electrochemistry, whether the

redox occurred at the metal center or the organic ligand. While it was generally known that the EPR technique could be helpful in answering some of these question directly, it was not appreciated for over three decades. This is likely because chemists have generally been reluctant to carry out in-depth studies on the paramagnetic materials since these compounds are not generally amenable to characterization by common instrumentation such as routine NMR spectroscopy and generally seen as 'spoiling their NMR'. Collaborations taking advantage of complementary chemical and EPR expertise have been useful and this has been facilitated by accessibility to high-field EPR instrumentation. In our case, collaboration began 15 years ago clearing uncertainties on Cr_2^{5+} and Mo_2^{5+} species. The *g*-values provided clear-cut evidence that the redox was metal-based and not ligand-centered, and confirming the number of suspected unpaired electrons on the complex via the Zero-field splitting and associated fine-structure transitions. The metal hyperfine structure showed directly that the bonding between the metal atoms was of a covalent type, involving the s, p and d orbitals, yielding their relative contributions by comparison with DFT calculations. Additionally, it has been learned that in many cases it is better to study dilute samples–compounds dissolved in nonreactive solvents–since they provide significantly better resolved spectral features than neat solid samples. For species that do not exhibit hyperfine structure, the spectral line widths provide additional information on the metal core as to whether the electrons are localized on one metal, both metal atoms or the entire molecular framework. Also shown is that in cases when EPR signals are expected but not observed when using commercially available (low-field, low-frequency) EPR spectrometers, high-field, high-frequency spectrometers can be invaluable. Facilities like NHMFL have reliable mechanisms to allow collaborations and are eager to serve the community. Even though this discussion focused on the value of EPR for dimetal paddlewheel complexes, there are multiple instances whereby analogies may be drawn by the inorganic chemistry community and beyond.

Acknowledgements

CAM thanks Texas A&M University and the National Science Foundation (IR/D support) while NSD thanks the NHMFL for providing access to HF-EPR over the years; the NHMFL is supported by the NSF Cooperative Agreement No. DMR-0654118 and by the State of Florida. We also acknowledge the work of our co-authors whose names appear in the references.

BIOGRAPHICAL INFORMATION

Naresh S. Dalal received his education at Panjab University, India, and the University of British Columbia (UBC), Canada. After postdoctoral work as a Killam Fellow at UBC, IBM Research and NRCC (Ottawa), he joined West Virginia University and became the Centennial Professor. He is currently at FSU as the Dirac Professor and the Robert O. Lawton Distinguished Professor. He is a Fellow of the AAAS, APS and ACS. He is interested in developing high-field EPR and NMR with applications in materials science.

Carlos A. Murillo studied chemistry at the Universidad de Costa Rica (UCR) and then Texas A&M University (TAMU) where he worked with F. Albert Cotton. After a postdoctoral stay with Prof. Malcolm Chisholm at Princeton University, he went back to the UCR where he became a full professor. He then moved to TAMU and eventually to the US National Science Foundation. He is a member of the Costa Rican Academy of Sciences, a fellow of the AAAS and is interested in compounds with metal-to-metal bonds.

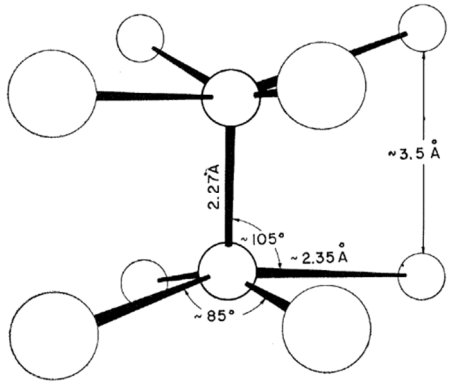

Fig. 1 The structure of the $[Re_2Cl_8]^{2-}$ anion as published in *Science* (ref 1).

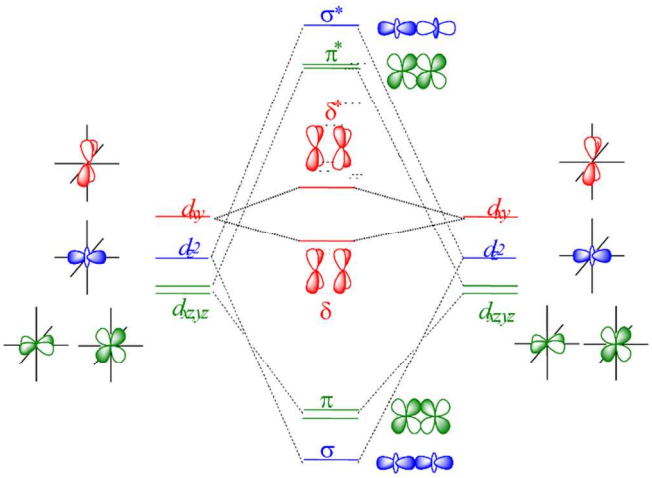

Fig. 2 Schematic molecular orbital diagram for a D_{4h} species with two metal atoms such as that in the quadruple bonded $[Re_2Cl_8]^{2-}$ anion that has 8 electrons.

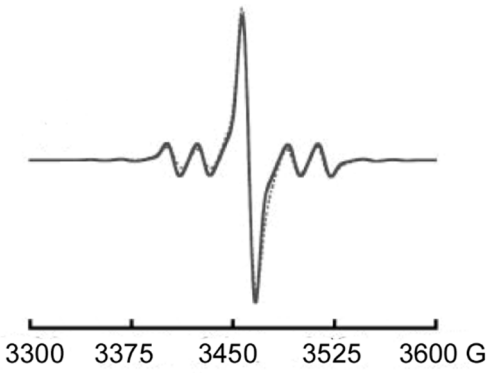

Fig. 3 X-band EPR spectrum of $[Mo_2(DAniF)_4]TiPB$. The solid line represents the experimental value and the dotted line is the simulated spectrum which is essentially identical with the experimental one.

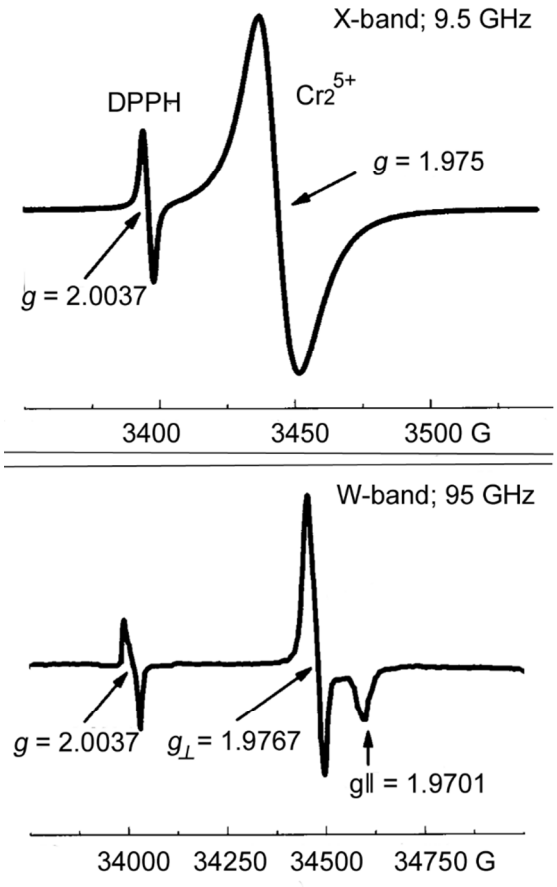

Fig. 4 Room temperature EPR spectra of solid $[Cr_2(DPPC)_4]PF_6$ using X-band (9.5 GHz, top) and W-band (95 GHz, bottom) frequencies. Signals on the left are from the organic free DPPH and those on the right from the dichromium species, illustrating the higher resolution afforded by the higher frequency (95 GHz), and the evidence that the unpaired electron is metal-centered.

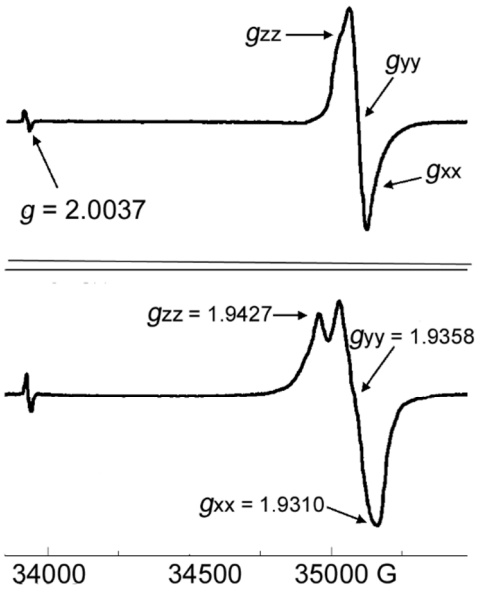

Fig. 5 The W-band spectra of $[Mo_2(TiBP)_4]PF_6$ powder at 300 (top) and 10 K (bottom).

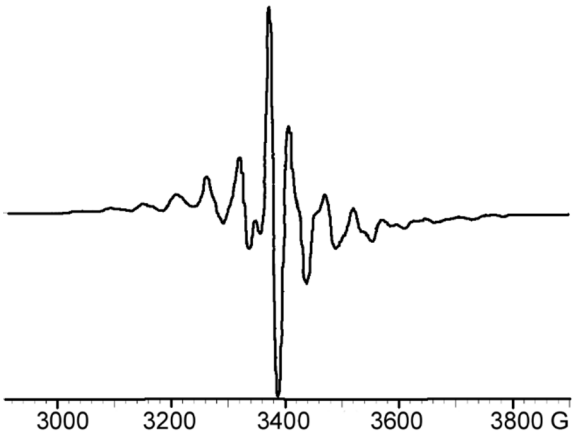

Fig. 6 The X-band EPR spectrum of the uncommon anionic species $[K(18\text{-crown-6})(THF)_2]V_2(DPhF)_4$ with a rare V_2^{3+} core taken at 6 K in a THF glass.

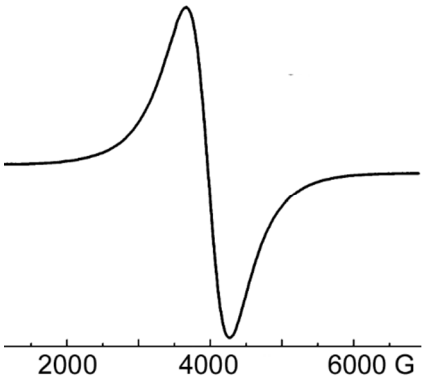

Fig. 7 X-band spectrum of $[Re_2(hpp)_4Cl_2]PF_6$ powder taken at ambient temperature consisting of a single exchange narrowed featureless line at g = 1.7421.

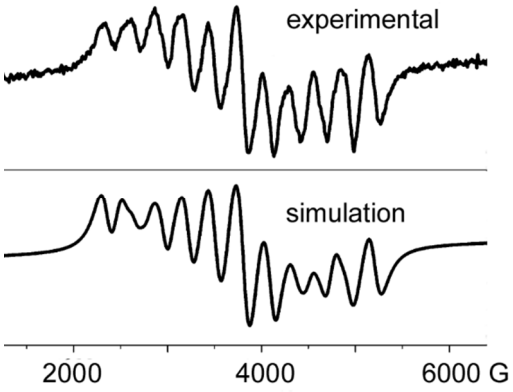

Fig. 8 The X-band spectrum of $Re_2(hpp)_4Cl_2]PF_6$ obtained in a 10 mM solution in CH_2Cl_2 placed in a sealed tube at 340 K. Above is the experimental spectrum and below is a simulation.

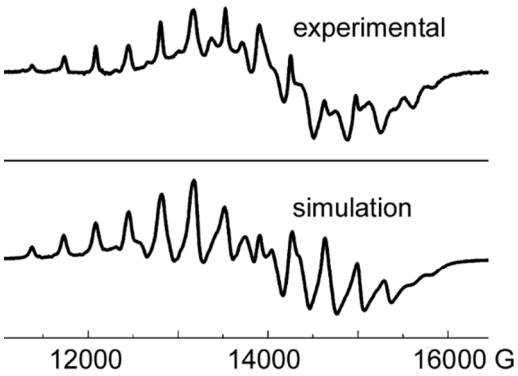

Fig. 9 The Q-band spectrum (34.5 GHz) of $[Re_2(hpp)_4Cl_2]PF_6$ obtained in CH_2Cl_2 frozen glass at 153 K. This spectrum is to be contrasted with that in Fig. 7, showing that the higher resolution can be obtained by utilizing dilute (mM) frozen solutions as compared to a neat powder.

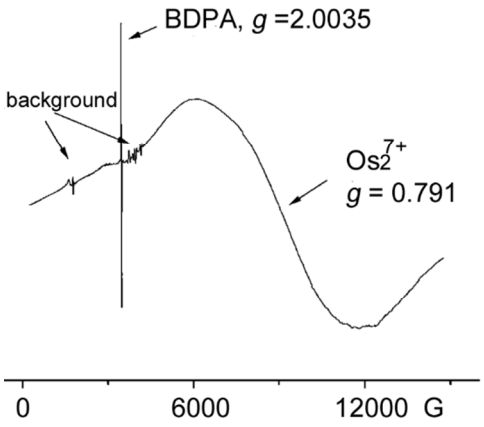

Fig. 10 The X-band (9.72754 GHz) spectrum of $[Os_2(hpp)_4Cl_2]PF_6$ collected from a solid sample at 6.5 K using the organic radical BDPA as internal reference. Note the large contrast in the line width of the organic radical and the diosmium species.

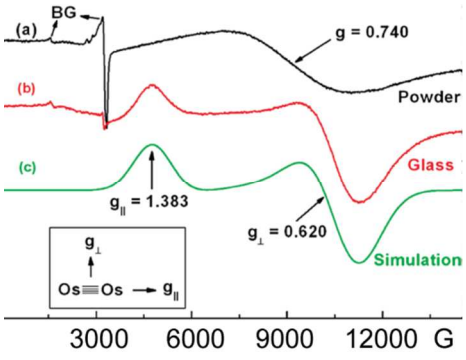

Fig. 11 (a) EPR spectrum of the powder of $[Os_2(hpp)_4Cl_2]PF_6$ at 6 K and at X-band (~9.4 GHz). (b) X-band EPR spectrum of the frozen glass of $[Os_2(hpp)_4Cl_2]PF_6 \cdot 2$acetone at 15 K. (c) The simulation of the frozen glass EPR spectrum in (b). The inset shows the orientations of *g* components relative to the Os–Os bond. BG denotes background.

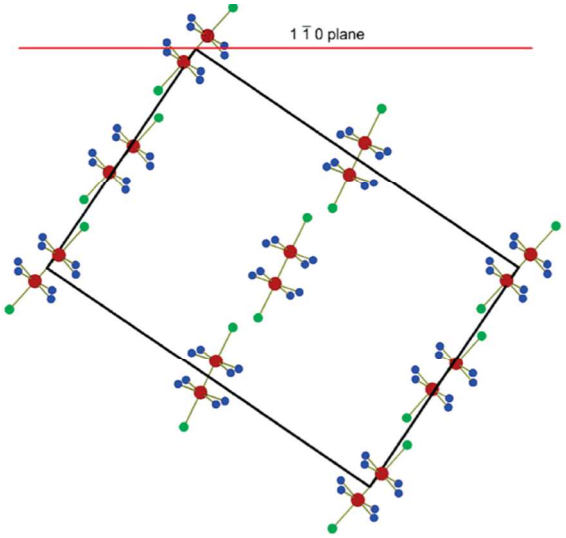

Fig. 12 The orientation of the unit cell of $[Os_2(hpp)_4Cl_2]PF_6 \cdot 2$acetone relative to the crystal axes. The Os–Os bonds lie with an angle of 8.835□ to the orthogonal plane. There are two magnetically distinct molecules in the unit cell clearly seen in the following figure.

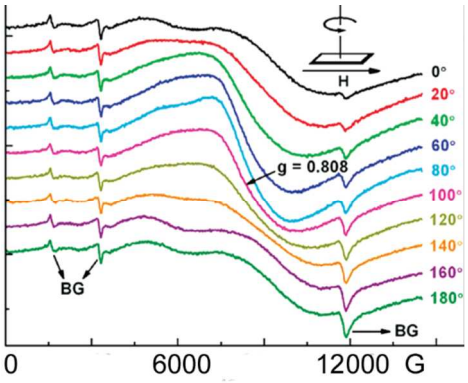

Fig. 13 Angular dependence of the crystal of $[Os_2(hpp)_4Cl_2]PF_6 \cdot 2$acetone at 4.5 K. The inset shows how the plate-like crystal was rotated by keeping the magnetic field in the plane of the plate-like crystal. Only a selected set of spectra are shown even though the measurements were done at 10□ intervals. BG denotes background.

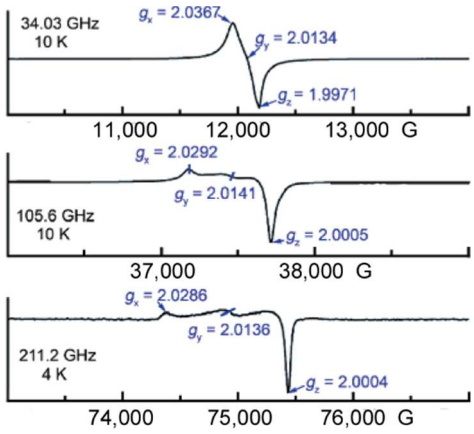

Fig. 14 Comparison of EPR spectra of $[Pd_2(DAniF)_4]PF_6$ at 34.03, 105.6, and 211.2 GHz (as marked) at cryogenic temperatures. Note the splitting of the peak into three *g* tensor components, ranging from 2.0004 to 2.0290. The slightly smaller *g* values at 34 GHz relative to those at 105.6 and 211.2 GHz are ascribed to an incomplete peak resolution and to a lesser extent to residual order-disorder effects related to a possible phase transition.

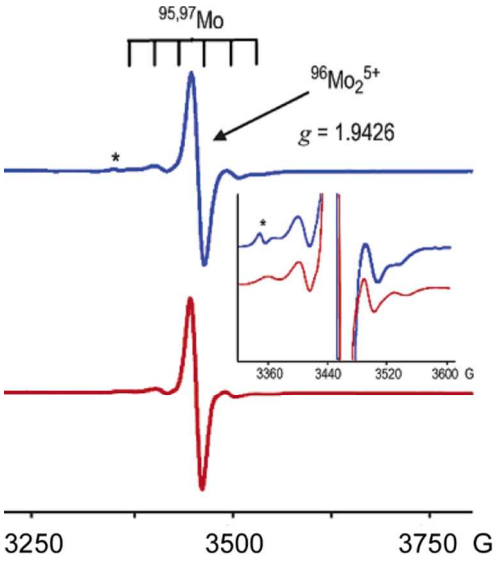

Fig. 15 X-band EPR spectrum at room temperature of a powdered sample of the *pairs-of-pairs* $[(DAniF)_3Mo_2(OCH_3)_2Zn(OCH_3)_2Mo_2(DAniF)_3]PF_6$ (top). The simulated spectrum using a g_{iso} of 1.9426, $A_{\square}$ = 37.7 G, and $A_{\perp}$ = 15.6 G is given below the experimental spectrum. The inset shows an enlargement to clarify the hyperfine peaks.

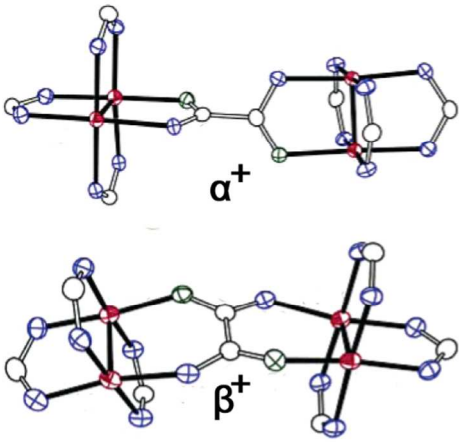

Fig. 16 The structures of the cations in the isomers α^+ and β^+ in $[(DAniF)_3Mo_2(ArN(O)CC(O)NAr)Mo_2(DAniF)_3]PF_6$, Ar = *p*-$MeOC_6H_4$. The hydrogen atoms in the methine carbon atom as well as the *p*-$MeOC_6H_4$ groups in the N atoms have been removed for simplicity. Color code: red = Mo, blue = N, white = C.

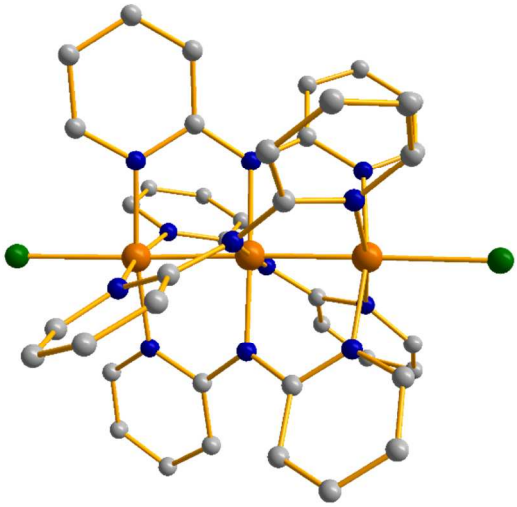

Fig. 17 The structure of the linear trinuclear $Cr_3(dpa)_4Cl_2$ compound. The chromium atoms are copper colored and the axial chlorine atoms green; nitrogen atoms are represented in blue.

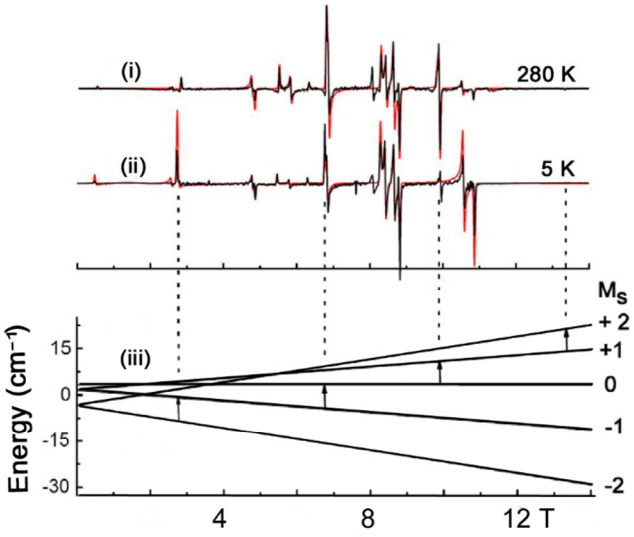

Fig. 18 EPR spectra of a powder of the linear trichromium compound $Cr_3(dpa)_4Cl_2$ taken at (i) 280 K and (ii) 5 K. The black trace corresponds to the experimental spectra while the red one to the simulated spectra. In the lower section (iii) the energy levels for H//z direction are provided. Peaks highlighted by arrows belong to the principal symmetry direction of the trichromium chain (z axis). The remaining features correspond to transitions for the perpendicular directions (x and y) of the Zero-field splitting tensor.

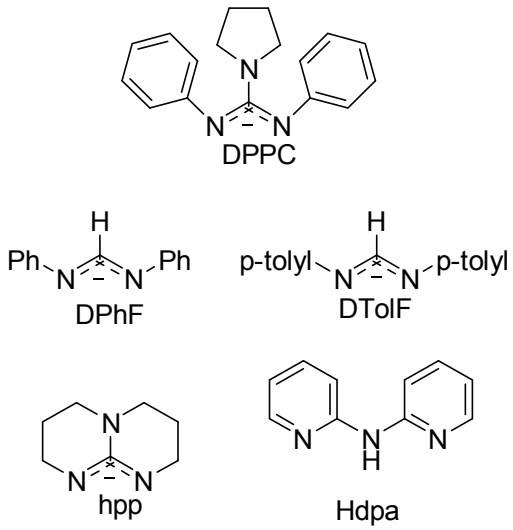

Scheme 1 Some of the ligands mentioned in the text.

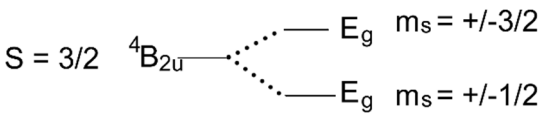

Scheme 2 Electronic splitting diagram for an 11 metal-centered species with idealized D_{4h} symmetry and a $\sigma^2\pi^4\delta^2\pi^2{*}\delta{*}$ electronic configuration.

Notes and references

(1) F. A. Cotton, N. F. Curtis, C. B. Harris, B. F. G. Johnson, S. J. Lippard, J. T. Mague, W. R. Robinson and J. S. Wood, *Science*, 1964, **145**, 1305–1307.
(2) One could also use d_{xy} orbitals but obviously not both at the same time.
(3) For example, see: F. A. Cotton, C.A. Murillo and R. A. Walton, Eds., in *Multiple Bonds between Metal Atoms*, 3rd ed. Springer Science and Business Media, Inc., New York, 2005.
(4) Compounds having paddlewheel structures but with weak or no metal–metal bonding such as dinuclear copper acetate are not considered here.
(5) In some areas, for example in organic chemistry, the use of ESR (electron spin resonance) is more common than EPR. Here we will use EPR.
(6) F. A. Cotton and E. Pedersen, *Inorg. Chem.*, 1975, **14**, 399–400.
(7) F. A. Cotton, E. A. Hillard and C. A. Murillo, *Inorg. Chem*., 2002, **41**, 1639–1644.
(8) Note that 1 cm^{-1} = 1 tesla = 10^4 gauss. Hf couplings are given in units of 10^{-4} cm^{-1}.
(9) F. A. Cotton, J. P. Donahue, C. A. Murillo, P. Huang and D. Villagrán, *Z. Anorg. Allg. Chem*., 2005, **631**, 2606–2612.
(10) This and all other figures showing EPR data are reproduced with slight modifications from those in the appropriate reference.
(11) A difference in the first decimal place in a *g* value is significant.
(12) F. A. Cotton, B. A. Frenz, E. Pedersen and T. R. Webb, *Inorg. Chem*., 1975, **14**, 391–398.
(13) I.-J. Chang and D. G. Nocera, *J. Am. Chem. Soc*., 1987, **109**, 4901–4907.
(14) (a) F. A. Cotton, L. M. Daniels, P. Huang and C. A. Murillo, *Inorg. Chem*., 2002, **41**, 317–320; (b) F. A. Cotton, N. S. Dalal, E. A Hillard, P. Huang, C. A. Murillo and C. M. Ramsey, *Inorg. Chem*., 2003, **42**, 1388–1390.
(15) Note that in an idealized tetragonal species, the direction along the metal-to-metal bond is unique while the two perpendicular directions are degenerate, thus the origin of the formula $g_{iso} = 1/3(g_{//} + 2g_{\perp})$.
(16) (a) F. A. Cotton, E. A. Hillard and C. A. Murillo, *J. Am. Chem. Soc*., 2003, **125**, 2026-2027; (b) F. A. Cotton, E. A. Hillard, C. A. Murillo and X. Wang, *Inorg. Chem*., 2003, **42**, 6063–6070.
(17) As noted in the ESI, the number of peaks for the hyperfine splitting is given by $2nI+1$ where n = number of atoms of a given type and I is the nuclear spin. Thus, for two vanadium centers with I = 7/2 one would expect (2x2x3.5)+1 = 15 lines.
(18) (a) F. A. Cotton and E. Pedersen, *J. Am. Chem. Soc*., 1975, **97**, 303–308; (b) F. A. Cotton, L. W. Shive and B. R. Stults, *Inorg. Chem*., 1976, **15**, 2239–2244.
(19) F. A. Cotton, J. P. Donahue, D. L. Lichtenberger, C. A. Murillo and D. Villagrán, *J. Am. Chem. Soc*., 2005, **127**, 10808–10809.
(20) (a) F. A. Cotton, N. E. Gruhn, J. Gu, P. Huang, D. L. Lichtenberger, C. A. Murillo, L. O. Van Dorn and C. C. Wilkinson, *Science*, 2002, **298**, 1971–1974; (b) G. M. Chiarella, F. A. Cotton, J. C. Durivage, D. L. Lichtenberger and C. A. Murillo, *J. Am. Chem. Soc*., 2013, **135**, 17889–17896.
(21) F. A. Cotton, N. S. Dalal, P. Huang, S. A. Ibragimov, C. A. Murillo, P. M. B. Piccoli, C. M. Ramsey, A. J. Schultz, X. Wang and Q. Zhao, *Inorg. Chem*., 2007, **46**, 1718–1726.
(22) J. F. Berry, F. A. Cotton, P. Huang and C. A. Murillo, *Dalton Trans*., 2003, 1218–1219.
(23) F. A. Cotton, N. S. Dalal, P. Huang, C. A. Murillo, A. C. Stowe and X. Wang, *Inorg. Chem*., 2003, **42**, 670–672.
(24) F. A. Cotton, G. M. Chiarella, N. S. Dalal, C. A. Murillo, Z. Wang and M. D. Young, *Inorg. Chem*., 2010, **49**, 319–324.
(25) F. A. Cotton and E. Pederson, *Inorg. Chem*., 1975, **14**, 383–387.
(26) F. A. Cotton, L. M. Daniels, A. Davison and C. Orvig, *Inorg. Chem*., 1981, **20**, 3051–3055.
(27) (a) P. A. Koz'min and G. N. Novitskaya, *Russ. J. Inorg. Chem*., 1972, **17**, 1652–1653; (b) F. A. Cotton and L. W. Shive, *Inorg. Chem*., 1975, **14**, 2032–2035.
(28) (a) F. A. Cotton and W. K. Bratton, *J. Am. Chem. Soc*., 1965, **87**, 921–921; (b) W. K. Bratton and F. A. Cotton, *Inorg. Chem*., 1970, **9**, 789–793.
(29) J. F. Berry, E. Bothe, F. A. Cotton, S. A. Ibragimov, C. A. Murillo, D. Villagrán and X. Wang, *Inorg. Chem*., 2006, **45**, 4396–4406.

(30) J. F. Berry, E. Bill, E. Bothe, F. A. Cotton, N. S. Dalal, S. A. Ibragimov, N. Kaur, C. Y. Liu, C. A. Murillo, S. Nellutla, J. M. North and D. Villagrán, *J. Am. Chem. Soc*., 2007, **129**, 1393–1401.
(31) F. A. Cotton, C. Lin and C. A. Murillo, *Inorg. Chem*., 2000, **39**, 4574–4578.
(32) L.-P. He, C.-L. Yao, M. Naris, J. C. Lee, J. D. Korp, J. L. Bear, *Inorg. Chem*., 1992, **31**, 620–625.
(33) For example, see: (a) F. A. Cotton, C. A. Murillo, J. H. Reibenspies, D. Villagrán, X. Wang and C. C. Wilkinson, *Inorg. Chem*., 2004, **43**, 8373–8378. (b) P. Angaridis, F. A. Cotton, C. A.; Murillo, D. Villagrán and X. Wang, *J. Am. Chem. Soc*., 2005, **127**, 5008–5009.
(34) W.-Z. Cheng, F. A. Cotton, N. S. Dalal, C. A. Murillo, C. M. Ramsey, T. Ren and X. Wang, *J. Am. Chem. Soc*., 2005, **127**, 12691–12696.
(35) In general, for large values of *D* and *S* = $^3/_2$, the effective (g^e) and actual *g*-values are related by $g_\perp = g_\perp^e/2$ and $g_\parallel = g_\parallel^e$. See R. J. Pilbrow, *J. Mag. Res*., 1978, **31**, 479–490. In addition $g_{iso} = (2g_\perp + g_\perp)/3$.
(36) F. A. Cotton and E. Pedersen, *Inorg. Chem*., 1975, **14**, 388–391.
(37) For example, see: (a) F. A. Cotton, C. Lin and C. A. Murillo, *Acc. Chem. Res*., 2001, **34**, 759–771; (b) F. A. Cotton, C. Lin and C. A. Murillo, *Proc. Natl. Acad. Sci. USA*, 2002, **99**, 4810–4813; (c) M. H. Chisholm and A. M. Macintosh, *Chem. Rev.*, 2005, **105**, 2949–2976.
(38) For example, see: (a) C. Creutz, P. C. Ford and T. J. Mayer, *Inorg. Chem*., 2006, **45**, 7059–7068; (b) A. Stebler, J. H. Ammeter, U. Füerholz and A. Ludi, *Inorg. Chem*., 1984, **23**, 2764–2767; (c) B. C. Bunker, R. S. Drago, D. N. Hendrickson, R. M. Richman and S. L. Kessel, *J. Am. Chem. Soc*., 1978, **100**, 3805–3814.
(39) F. A. Cotton, N. S. Dalal, C. Y. Liu, C. A. Murillo, J. M. North and X. Wang, *J. Am. Chem. Soc*., 2003, **125**, 12945–12952.
(40) The comproportionation constant is defined as
$K_C = e^{\Delta E_{1/2}/25.69}$, where $\Delta E_{½}$ is the difference in electrode potential between two consecutive redox processes. The expression can be easily derived from the thermodynamic relationships: $\Delta G = -RTlnK = -n\mathcal{F}E$.
(41) F. A. Cotton, C. Y. Liu, C. A. Murillo and Q. Zhao, *Inorg. Chem*., 2007, **46**, 2604–2611.
(42) For example, see: F. A. Cotton, C. A. Murillo, M. D. Young, R. Yu and Q. Zhao, *Inorg. Chem*., 2008, **47**, 219–229.
(43) F. A. Cotton, L. M. Daniels, C. A. Murillo and I. Pascual, *J. Am. Chem. Soc*., 1997, **119**, 10223–10224.
(44) J. F. Berry, F. A. Cotton, T. Lu, C. A. Murillo, B. K. Roberts and X. Wang, *J. Am. Chem. Soc.*, 2004, **126**, 7082–7096.
(45) J. Wang, Z. Wang, R. J. Clark, A. Ozarowski, J. van Tol and N. S. Dalal, *Polyhedron*, 2011, **30**, 3058–3061.